Front. Environ. Sci. Eng., 2016, 10(4) : 12
DOI 10.1007/s11783-016-0855-9

RESEARCH ARTICLE

Effect of protein on PVDF ultrafiltration membrane fouling behavior under different pH conditions: interface adhesion force and XDLVO theory analysis

Xudong WANG[1], Miao ZHOU[1], Xiaorong MENG[1,2], Lei WANG (✉)[1], Danxi HUANG[1]

1 School of Environmental and Municipal Engineering, Xi'an University of Architecture and Technology, Xi'an 710055, China
2 School of Science, Xi'an University of Architecture and Technology, Xi'an 710055, China

HIGHLIGHTS

- pH values of the BSA solution significantly impact the process of membrane fouling.
- Dramatic flux decline is caused by membrane – BSA adhesion force at start of filtration.
- XDLVO theory shows the polar or Lewis acid – base interaction plays a major role in membrane fouling.

GRAPHIC ABSTRACT

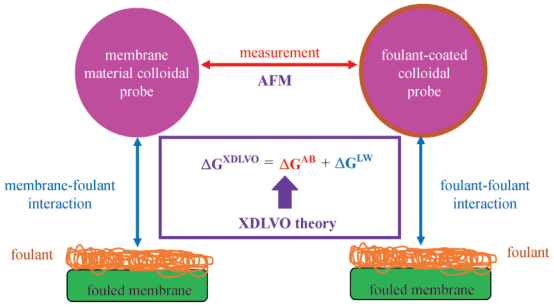

ARTICLE INFO

Article history:
Received 14 March 2016
Received in revised form 29 April 2016
Accepted 25 May 2016

Keywords:
PVDF membrane
Membrane fouling
Adhesion force
Protein
Interfacial free energy

ABSTRACT

To further determine the fouling behavior of bovine serum albumin (BSA) on different hydrophilic PVDF ultrafiltration (UF) membranes over a range of pH values, self-made atomic force microscopy (AFM) colloidal probes were used to detect the adhesion forces of membrane–BSA and BSA–BSA, respectively. Results showed that the membrane–BSA adhesion interaction was stronger than the BSA–BSA adhesion interaction, and the adhesion force between BSA–BSA-fouled PVDF/PVA membranes was similar to that between BSA–BSA-fouled PVDF/PVP membranes, which indicated that the fouling was mainly caused by the adhesion interaction between membrane and BSA. At the same pH condition, the PVDF/PVA membrane–BSA adhesion force was smaller than that of PVDF/PVP membrane–BSA, which illustrated that the more hydrophilic the membrane was, the better antifouling ability it had. The extended Derjaguin–Landau–Verwey–Overbeek (XDLVO) theory predicts that the polar or Lewis acid–base (AB) interaction played a dominant role in the interfacial free energy of membrane–BSA and BSA–BSA that can be affected by pH. For the same membrane, the pH values of a BSA solution can have a significant impact on the process of membrane fouling by changing the AB component of free energy.

1 Introduction

Ultrafiltration (UF) technology is considered one of the most promising new water treatment technologies in the 21st century [1]. However, membrane fouling is still a major obstacle for the wider use of UF technology [2,3]. Membrane fouling is due to the physical and chemical effects of various pollutants and membrane interfaces in the filtration process. The behavior of the pollutants on the membrane interface is not only related to the property of the membrane, but also to the chemical conditions of a solution such as pH, ionic strength and the coexistence of metal ions [4]. Previous studies have shown that the

✉ Corresponding author
E-mail: wl0178@126.com

reduction in pH could reduce the molecular size of natural organic matter (NOM) and enhance the adsorption onto membrane, resulting in significant fouling [5,6].

Recent research results indicate that the interfacial property of membranes have an important impact on the accumulation of membrane fouling [7]. Chang et al. also think that the surface property of a membrane has an important impact on the membrane–foulant interactions [8].The interactions between membrane and foulant will affect the adsorption of foulant on the surface of the membrane. To further clarify the organic fouling behavior of membranes, Wang et al. used atomic force microscopy (AFM) with a self-made polyvinylidene fluoride (PVDF) colloidal probe and a foulant-coated colloidal probe [9]. The result indicated that the membrane–foulant adhesion force was much stronger than the foulant–foulant interaction force. They found a positive correlation between the membrane–foulant adhesion force and the flux decline rate and extent in the initial filtration stage.

Protein is one of the major membrane foulants [10–12] known to cause significant loss of membrane permeability and is often used as a representative contaminant to analyze the mechanism of membrane fouling [13]. The ionic strength and pH of a solution will have a huge impact on the protein molecular structure and membrane surface charge because protein is an amphoteric substance [14]. Thus, the separation process of the protein in a UF membrane must be a dynamic and complex process. Therefore, the study of the UF membrane separation process and influencing factors will provide a better understanding of the membrane fouling mechanism, and will help us to effectively control membrane fouling.

Previous studies on the membrane fouling mechanism for protein have been at the macroscopic level [15,16]. The transmembrane pressure and the membrane flux decline rate were used to characterize protein fouling during constant flux dead-end microfiltration [17]. Ma et al. used membrane flux decline rate and membrane porosity to analyze membrane fouling by low-dose aluminum coagulation with BSA [18]. People began to think about and explore the microscale and microenvironment interface problem [19,20]. AFM provides an effective means for the determination of microscopic interaction forces between foulant and membranes. In recent years, AFM has been widely used because of its ability to quantitatively measure the interaction forces involved at the membrane–foulant and foulant–foulant interfaces [9,21]. Our previous studies have systematically investigated the applicability of the PVDF probe and the foulant-coated probe prepared with the aid of self-assembly devices in the assessment of membrane fouling [22].

The extended Derjaguin–Landau–Verwey–Overbeek (XDLVO) theory can describe the attachment of a colloidal particle to a surface because of three interactions (as membrane fouling contributors): Lifshitz–van der Waals (LW), polar or Lewis acid–base (AB) and electrostatic double-layer free energies (EL) [23–25]. Our previous study analyzed the UF process for humic acid (HA). We measured the adhesion forces of membrane–HA and HA–HA by AFM and calculated the surface interaction energy with the XDLVO theory, which could explain the effect and regularity of HA solution pH and the hydrophilicity of the PVDF UF membrane interface on the membrane fouling behavior. The results showed that the membrane–HA interfacial free energy of adhesion and the AB interactions played an important role in the occurrence of membrane fouling and demonstrated that the XDLVO theory could reveal the essential reason for membrane fouling behavior and its influence rules of HA on the particular membrane interface at different pH values [26].

In this paper, BSA was used as a typical protein contaminant. The adhesion forces of membrane–BSA and BSA–BSA were measured by AFM and the surface interaction energy was calculated using the XDLVO theory to predict the membrane behavior and fouling mechanism of BSA on a PVDF UF membrane interface in solutions with different pH values; measurements were also taken to provide a theoretical basis for the operation of the regulation and control of the UF membrane fouling processes.

2 Materials and methods

2.1 Preparation of the PVDF UF membrane

The flat sheet PVDF UF membranes used in this study were prepared via the nonsolvent-induced phase separation method as follows. Polyvinylalcohol (PVA, 18–99, Sigma-Aldrich, USA) or polyvinylpyrrolidone (PVP, K30, BASF, Germany) were mixed with polyvinylidene fluoride (PVDF, Solef® 6020 Solvay Co, USA), LiCl (AR, Kermel, Tianjin, China), anhydrous alcohol (AR, Kermel, Tianjin, China) and N,N-dimethylactamide (DMAc, >99%, Kermel, Tianjin, China) for 16–24 h at 60°C in a vessel equipped with a stirrer [27]. The compositions of different casting solutions of blending membranes were signed as PVDF/PVA and PVDF/PVP membranes, respectively. The composition of the casting solution as regards PVDF/PVA and PVDF/PVP is shown in Table 1. The compositions of different casting solutions of blending

Table 1 Compositions of different casting solution

compositions/%	PVDF/PVA	PVDF/PVP
PVDF	17	17
PVA	3	0
PVP	0	3
PEG	3	0
LiCl	3	3
DMAc	74	77

membranes were signed as PVDF/PVA and PVDF/PVP membranes, respectively.

2.2 Preparation of BSA solution

The bovine serum protein BSA (*Mw* = 67000 Da, Sigma-Aldrich, USA) was chosen to represent the protein-like substance in natural organic matter. The BSA solution (1 $g \cdot L^{-1}$) was prepared by dissolving 1 g BSA into 1000 mL deionized water. The BSA solution was stirred for 12 h at room temperature and then filtered through a 0.45 μm microfiltration membrane. The solution was stored at 4°C. In the experiment, the BSA solution was diluted to a concentration of 20 $mg \cdot L^{-1}$ and the pH values were adjusted to 3, 4.7 and 9 by addition of 0.1 $mol \cdot L^{-1}$ HCl or 0.1 $mol \cdot L^{-1}$ NaOH, as needed.

2.3 UF experiment and analysis of membrane fouling behavior

Laboratory-scale dead-end membrane filtration equipment (an SCM cup-shaped stirred cell, Institute of Physics, Chinese Academy of Sciences) with an effective membrane filtration area of 33.2 cm^2 was used to verify the effect of the pH value of the BSA solution. For each filtration experiment, the membrane was stabilized with deionized water for 0.5 h to establish a stable permeate flux in 100 kPa by N_2. Next, BSA solution was filtrated and the permeability for BSA solution was measured for 2 h. To carry out a comprehensive evaluation of the experimental data, the J/J_0 was used to represent the flux in each condition.

2.4 Preparation of colloidal probes

The colloidal probes used in this experiment were based on our previous PVDF microparticle probes [9,26]. The measurement of the interfacial adhesion force between the membrane and BSA was made using a self-made PVDF membrane material probe. The preparation method was as follows: a two-component epoxy resin (1:1) was used to glue SiO_2 particles (4–5 μm in diameter) to a commercial V-shaped nonconductive silicon nitride tip-less AFM cantilever end (NP-010, Bruker, Germany) with the aid of an optical microscope (TH4-200; Olympus, Japan). Then, the probe was placed in a heating station for 30 min (60°C–80°C), and cooled in air to room temperature. The casting solutions (in this experiment the casting solution was PVDF/PVP or PVDF/PVA) were diluted 5 times with DMAc. The SiO_2 microsphere was dipped into diluted casting solution for 15–20 s and immersed into ultrapure water to ensure full replacement of the solvent. Thus, the membrane-coated probe was prepared.

The preparation method used for the BSA-coated probe for the measurement of the BSA–BSA interfacial adhesion force was as follows. The prepared membrane-coated colloidal probes were immersed in the BSA solution (which was the same as the test fouling BSA solution) for 24 h and were then stored at room temperature before use. Fig. S1 shows the representative SEM images of modified AFM colloidal probes (see Supplementary material).

2.5 Measurement of surface morphology, roughness and interfacial adhesion force

Another scanning electron microscope (SEM, JSM5800, Japan) was used to obtain images of clean and BSA-fouled membranes. A MultiMode 8.0 AFM (Bruker, Germany) instrument was used to measure the surface morphology of original and BSA-fouled membranes in contact mode with an AFM probe (spring constant = 0.12 $N \cdot m^{-1}$). The scan area was 10 μm × 10 μm at 512 × 512 pixels. The roughness parameter used in this study is defined as the mean roughness, Ra. The interfacial adhesion forces of membrane–BSA and BSA–BSA were measured in a liquid environment using the contact mode with colloidal probes. Before each measurement, the sample cell was washed three times with ultrapure water and once with the test solution. Each measurement was conducted at 10–15 different points on every membrane at least, and 10 force measurements were taken at each location. The probability distribution of the force measurements at pH 4.7 is shown in Fig. S2 (see Supplementary material). To ensure the accuracy of the measurement, the integrity of the colloidal probe was inspected by SEM before and after each test.

2.6 The XDLVO theory

The XDLVO theory can describe the attachment of a colloidal particle to a surface as a result of three interactions [23,24]. The total interfacial free energy of adhesion is given by [28]:

$$\Delta G^{XDLVO} = \Delta G^{LW} + \Delta G^{AB} + \Delta G^{EL}, \quad (1)$$

where ΔG^{LW}, ΔG^{AB} and ΔG^{EL} represent the Lifshitz–van der Waals (LW), polar or Lewis acid–base (AB) and electrostatic double-layer free energies (EL), respectively. The values of ΔG^{XDLVO} represent the interfacial free energy between membrane and BSA or BSA and BSA. If the value is negative, it indicates that the two are attracted to each other, here, the smaller the value the more intense is the attraction, and the more serious is the membrane fouling. If the value is positive, it indicates that the two are mutually exclusive, here, the greater the value the more intense is the rejection, and the lighter is the membrane fouling.

Because the ΔG^{EL} has a small impact on the surface free energy, only the LW and AB interaction components can be used to analyze membrane fouling [29]. Therefore, the calculation formula of the total interfacial free energy of adhesion can be simplified as follows [28]:

$$\Delta G^{XDLVO} = \Delta G^{LW} + \Delta G^{AB}. \quad (2)$$

The calculation formula of the LW and AB interaction can be given as [28]:

$$\Delta G^{LW} = 2(\sqrt{\gamma_l^{LW}} - \sqrt{\gamma_m^{LW}})(\sqrt{\gamma_f^{LW}} - \sqrt{\gamma_l^{LW}}), \quad (3)$$

$$\Delta G^{AB} = 2\sqrt{\gamma_l^+}(\sqrt{\gamma_m^-} + \sqrt{\gamma_f^-} - \sqrt{\gamma_l^-}) + 2\sqrt{\gamma_l^-}(\sqrt{\gamma_m^+} + \sqrt{\gamma_f^+} - \sqrt{\gamma_l^+}) - 2(\sqrt{\gamma_m^+\gamma_f^-} + \sqrt{\gamma_m^-\gamma_f^+}), \quad (4)$$

where γ^{LW},γ_l^+,γ_i^- are the LW, the electron acceptor and the electron donor component, respectively. The γ^{LW},γ_l^+,γ_i^- can be calculated by the extended Young equation, which can be given as follows [28]:

$$(1+\cos\theta)\gamma_l^{TOT} = 2(\sqrt{\gamma_i^{LW}\gamma_l^{LW}} + \sqrt{\gamma_i^+\gamma_l^-} + \sqrt{\gamma_i^-\gamma_l^+}), \quad (5)$$

where θ is the contact angle, γ_l^{TOT},γ_l^{LW},γ_l^- and γ_l^+ can be obtained from Table 2 [28], and

$$\gamma_i^{TOT} = \gamma_i^{AB} + \gamma_i^{LW}, \quad (6)$$

$$\gamma_i^{AB} = 2\sqrt{\gamma_i^+\gamma_i^-}. \quad (7)$$

Contact angles were measured by the sessile drop method with hydrophilic contact angle measurements (Datpahysies-OCA20). Before measurement, the membrane samples were submerged in deionized water at pH 3, 4.7 and 9 adjusted by hydrochloric acid and sodium hydroxide for at least 24 h. And the BSA samples were obtained by depositing the BSA solution at pH 3, 4.7 and 9 onto clean flat glass slides [30].

Table 2 Surface tension properties (mJ·m^{-2}) of probe liquids at 20°C

	γ_l^+	γ_i^-	γ^{LW}	γ^{AB}	γ^{TOT}
Ultrapure water	25.5	25.5	21.8	51.0	72.8
Diiodomethane	0.0	0.0	50.8	0.0	50.8
Glycerol	3.9	57.4	34.0	30.0	64.0

2.7 Measurement of zeta potential, particle size, membrane porosity and mean pore size

The zeta potential and mean size of BSA were measured with Malvern Zetasizer NanoZS90 (Malvern Instruments Limited, UK). Membrane porosity was determined by the gravimetric method, determining the weight of liquid (here, alcohol) contained in the membrane pores [31]. The mean pore size was evaluated using the flow rate method [32].

3 Results and discussion

3.1 The properties of the PVDF UF membrane

Figure 1 shows the FTIR data for the self-made PVDF/PVA and PVDF/PVP membranes, which had different properties. The characteristic absorption peaks of PVDF were at 1420, 1173, 1069 and 879 cm^{-1} [33]. The PVDF/PVA membrane has a peak at 3370 cm^{-1}, which is the stretching vibration absorption of –OH in PVA. While the PVDF/PVP membrane has the carbonyl group absorption peak, which is in PVP at 1676 cm^{-1}, there is no absorption peak at 3000 cm^{-1}. The measurement results showed that a number of additives such as PVA or PVP can be retained in the PVDF UF membrane in the process of phase separation. It can be supposed that different degrees of PVA and PVP would improve the hydrophilic properties of the PVDF UF membrane.

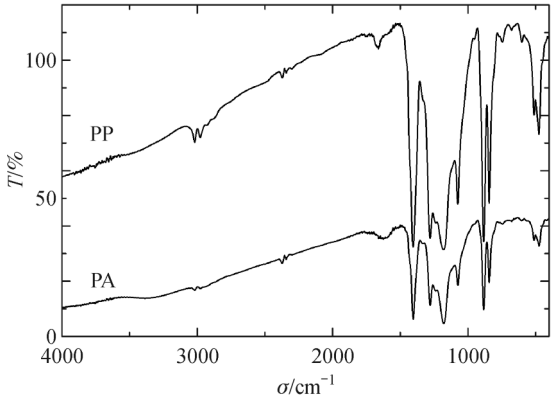

Fig. 1 FTIR spectra of PVDF/PVA and PVDF/PVP membranes

Table 3 shows the structure parameters of the self-made PVDF UF membranes that were used in the experiment. The pure water permeability and mean pore size of the PVDF/PVA and PVDF/PVP membranes have a similar average. The pure water permeability of PVDF/PVA and PVDF/PVP membranes was 258.62 and 308.82 LMH under 100 kPa by N_2, respectively. The mean pore sizes of the PVDF/PVA and PVDF/PVP membranes were 46.84 and 43.64 nm, respectively, but there were large differences in terms of their hydrophilic properties. The PVDF/PVA membrane was more hydrophilic (contact angle of

Table 3 PVDF UF membrane structure parameters

types	PVDF/PVA	PVDF/PVP
BSA rejection/%	89.2	78.5
porosity/%	62.9	78.5
mean pore size/nm	46.8	43.6
contact angle/(º)	62.7	69.8
flux/LMH	258.6	308.8

62.73º) than the PVDF/PVP membrane (contact angle of 69.82º). Addition of PVP increased the membrane porosity to 78.53%, while the porosity of the PVDF/PVA membrane was 62.91%. The BSA rejection of the PVDF/PVA and PVDF/PVP membranes was 89.20% and 78.51%, respectively. Thus, the PVDF/PVA membrane has a better BSA rejection.

3.2 Effect of pH on the physicochemical properties of BSA

Figure 2 shows the zeta potential and particle size curves of BSA solution at different pH values. When the pH was less than 4.7, the basic residues and hydrogen ions on the BSA surface were completely associative, and the zeta potential had a stable positive charge. When the pH was 4.7, the hydrogen ion on the BSA surface gradually dissociated, the zeta potential reduced to close to zero. The hydrated radius was the smallest and the particle size was also the smallest at this time. With a further increase in the pH value, amino acidic residues on the BSA surface gradually played a role in the solution, increasing the negative charge on the protein surface, while the zeta potential was negative and the negative charge increased significantly. When the amino acid residues on the surface completely dissociated, the zeta potential became stabilized [34]. It can be seen that the pH value change the properties of the protein surface charge by affecting the degree of protonation of amino acid residues on the protein surface.

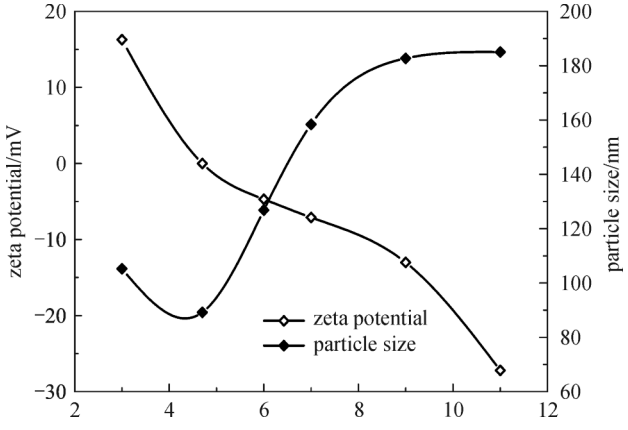

Fig. 2 Effect of BSA solution pH on zeta potential and particle size

3.3 Membrane flux in BSA UF

Figure 3 shows the flux decline curves of the PVDF/PVA and PVDF/PVP membranes in BSA solution at three different pHs, namely 3, 4.7 and 9. At different pH conditions, the flux decline rates of the PVDF/PVA membranes were lower than those of the PVDF/PVP membranes, and this was because of the PVDF/PVA membranes being more hydrophilic than the PVDF/PVP

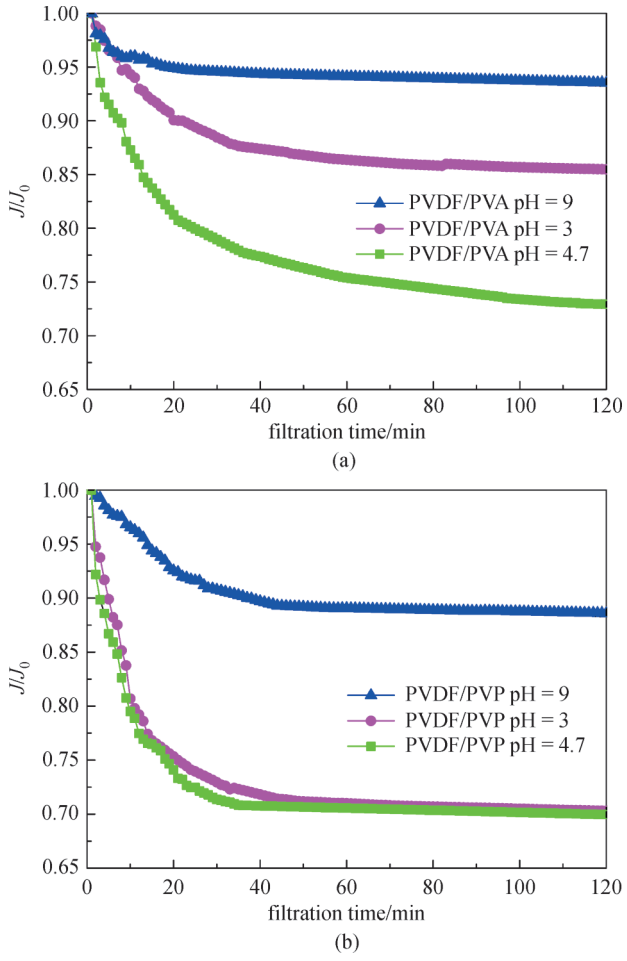

Fig. 3 Flux decline in BSA ultrafiltration at different pHs (a) is for PVDF/PVA, (b) is for PVDF/PVP)

membranes, thus having better antifouling ability for BSA. When the solution pH was alkaline, the flux decline rates of the PVDF/PVA and PVDF/PVP membranes were the lowest, and the membrane fouling was the lightest. When the solution pH was acidic, the PVDF/PVP membrane flux declined rapidly at the initial filtration stage, and when the pH was 4.7, the PVDF/PVA and PVDF/PVP membranes had the most serious decline in flux; the flux loss rate reached 30%. Then, the flux of the PVDF/PVA and PVDF/PVP membranes gradually achieved stability. This is because that the isoelectric point of BSA was at pH 4.7, the charge of BSA was close to zero and the flux decline rate of the two membrane materials increased. This indicated that an acidic solution environment would cause serious membrane fouling of BSA.

3.4 Analysis of the adhesion force of membrane–BSA and BSA–BSA

Figure 4 shows the effects of different pH values on the adhesion forces of PVDF/PVA membrane–BSA and BSA–

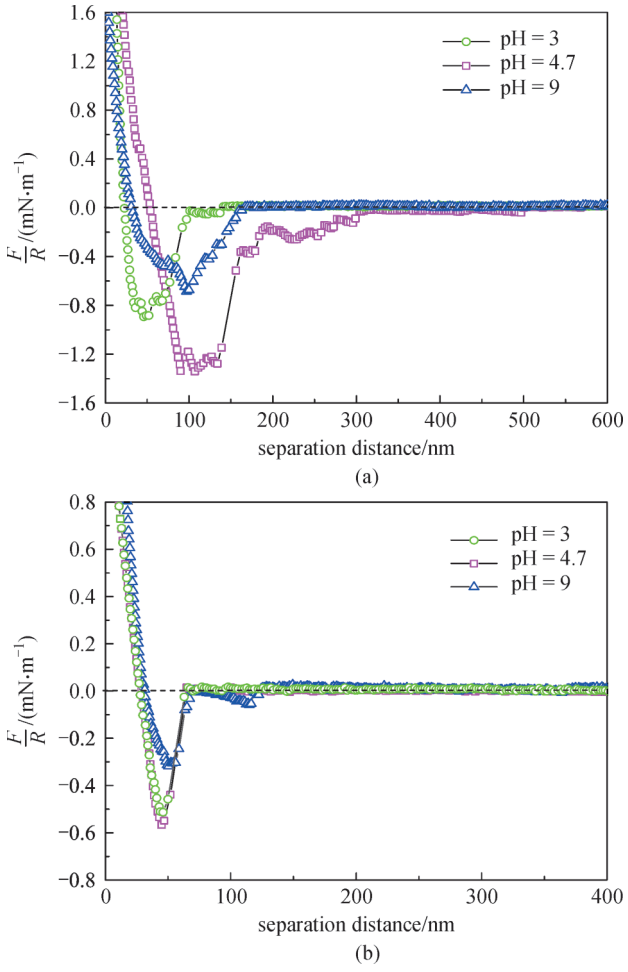

Fig. 4 Adhesion forces of PVDF/PVA membrane-BSA (a) and BSA-BSA (b)

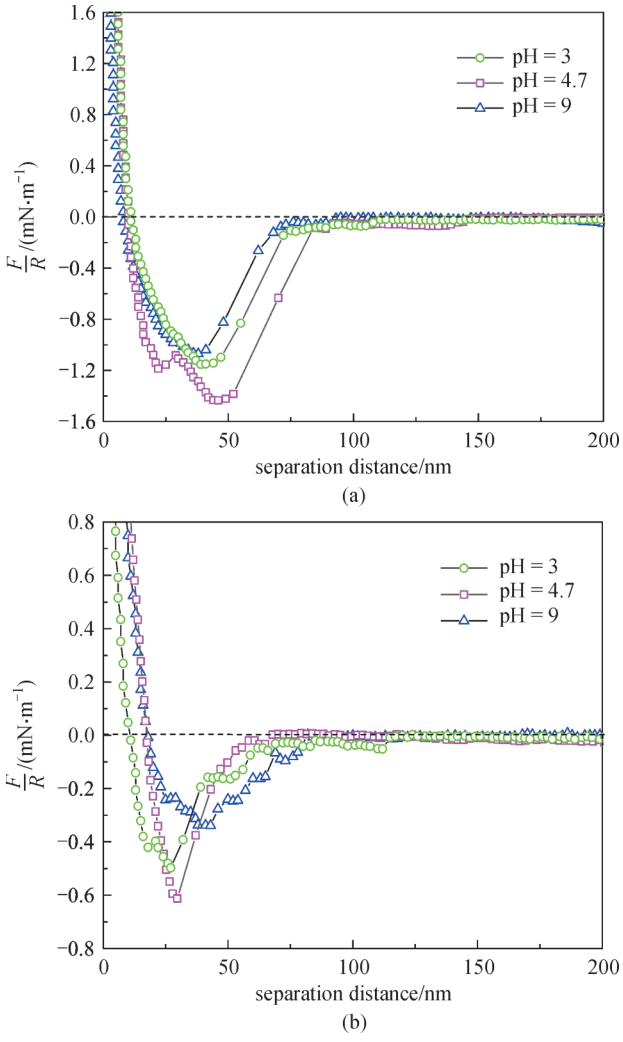

Fig. 5 Adhesion forces of PVDF/PVP membrane-BSA (a) and BSA-BSA (b)

BSA. When the pH values were 3, 4.7 and 9, the adhesion values of the PVDF/PVA membrane–BSA were 0.91, 1.35 and 0.74 mN·m^{-1}, respectively, whereas the adhesion values for BSA–BSA were 0.49, 0.56 and 0.31 mN·m^{-1}, respectively. Figure 5 shows the effects of different pH values on the adhesion of the PVDF/PVP membrane–BSA and the adhesion of BSA–BSA. When the pH was 3, 4.7 and 9, the adhesion values of the PVDF/PVP membrane–BSA were 1.24, 1.47 and 1.12 mN·m^{-1}, respectively, whereas for BSA–BSA they were 0.52, 0.61 and 0.34 mN·m^{-1}, respectively.

From Figs. 4 and 5, it is obvious that the adhesion forces of both the PVDF/PVA and PVDF/PVP membranes against BSA were stronger than the adhesion of BSA to itself. Combing with the result that the membrane flux declines dramatically at the beginning of filtration and gentlely decline in the later filtration stage (Fig. 3), it is obvious that the adhesion force of membrane–BSA was determined the membrane fouling at the initial filtration stage, whereas the BSA–BSA interaction force was closely related to the membrane fouling in the later filtration stage. Moreover, the membrane–BSA adhesion interaction was stronger than the BSA–BSA interaction, indicated that the fouling was mainly caused by the adhesion interaction between the membrane and the foulant. With increasing pH values, the adhesion interactions of PVDF/PVP membrane–BSA, PVDF/PVA membrane–BSA and BSA–BSA, all increased initially but then decreased; and when the pH increased to 4.7, the net charge on the BSA molecular surface was zero, the hydrated radius of BSA was smallest, zeta potential was zero. Therefore, at this time, the adhesion forces of both PVDF/PVA and PVDF/PVP membrane against BSA and BSA on BSA reached a maximum.

Our previous findings [9,22,26,35] show that the adhesion interaction between the foulants and the membrane determines the extent of membrane fouling in a separation process. When the micro-force was smaller, the membrane fouling was lighter, and the antifouling performance of the membrane was stronger. In contrast, the

antifouling performance of the membrane was poor. At the same pH condition (Figs. 4 and 5), the adhesion force between the PVDF/PVA membrane and BSA was smaller than that of PVDF/PVP membrane and BSA, which illustrated that the more hydrophilic the membrane, the better its antifouling ability. The adhesion force for BSA–BSA-fouled PVDF/PVA membranes was similar to that for BSA–BSA-fouled PVDF/PVP membranes. After a cake layer formed in the later filtration stage, membrane fouling was mainly affected by the adhesion interaction BSA–BSA, and the physical and chemical properties of membranes that have a strong effect in the initial filtration were less relevant. These results confirmed that elimination of the membrane–BSA adhesion force is important to control the protein fouling of membranes.

3.5 Microscopic morphology of the membrane

Figure 6 shows the surface SEM images of the clean membranes and membranes fouled by BSA solutions with different pH values. It is not difficult to find that some foulant was deposited on the surface of the PVDF/PVA and PVDF/PVP membranes after filtration with BSA solution at pH 3. This showed that the foulant adhered to the surface of the UF membrane, as some furrows can be seen in Fig. 6 that were formed by foulant. Compared with the original membrane, there was more foulant deposited on the membranes fouled by BSA solution at pH 4.7 than on the membranes that were fouled by BSA solution at pH 3. This indicated that the BSA solution at pH 4.7 could foul the PVDF UF membranes more seriously. It is obvious that PVDF/PVP membranes had serious membrane fouling. However, the morphology of clean membranes and of PVDF/PVA/PVDF/PVP membranes that were fouled by BSA solution at pH 9 were similar, illustrating that membrane fouling caused by BSA solution at pH 9 was the lightest.

Figure 7 shows three-dimensional AFM images of the original and BSA-fouled PVDF/PVA and PVDF/PVP membranes with pH values of 3, 4.7 and 9. The surfaces of the original PVDF/PVA and PVDF/PVP membranes were different. AFM images show that the Rq and Ra values of PVDF/PVA membranes were smaller than for PVDF/PVP membranes. The original PVDF/PVA membranes were smoother than the original PVDF/PVP membranes. This phenomenon might be related to the compatibility of components in casting solution and to the forming process of the membrane systems. Compared with the original membranes, the Rq and Ra values of PVDF/PVA membranes that were fouled by BSA solution at pH 3 sharply declined from 68.2 to 48.6 nm and from 54.2 to 35.1 nm, respectively. However, the Rq and Ra values of PVDF/PVP membranes fouled with BSA at pH 3 had a certain degree of increased roughness. This may be caused by adherence of small amounts of BSA to the membrane surface. The Rq and Ra values of PVDF/PVA membranes at pH 4.7 were smaller than at pH 3, but for PVDF/PVP membranes fouled with BSA at pH 4.7 the Rq and Ra values increased dramatically. While the adhesion value of the PVDF/PVA membrane–BSA at pH 4.7 (1.35 $mN \cdot m^{-1}$) was more than that at pH 3 (0.91 $mN \cdot m^{-1}$) from Fig. 4 (a). This phenomenon may be related to the structure and chargeability of the BSA molecules. The exact relationship between roughness and the degree of membrane fouling warrants further investigation in the future. The Rq and Ra values of clean PVDF/PVA/PVDF/PVP membranes that

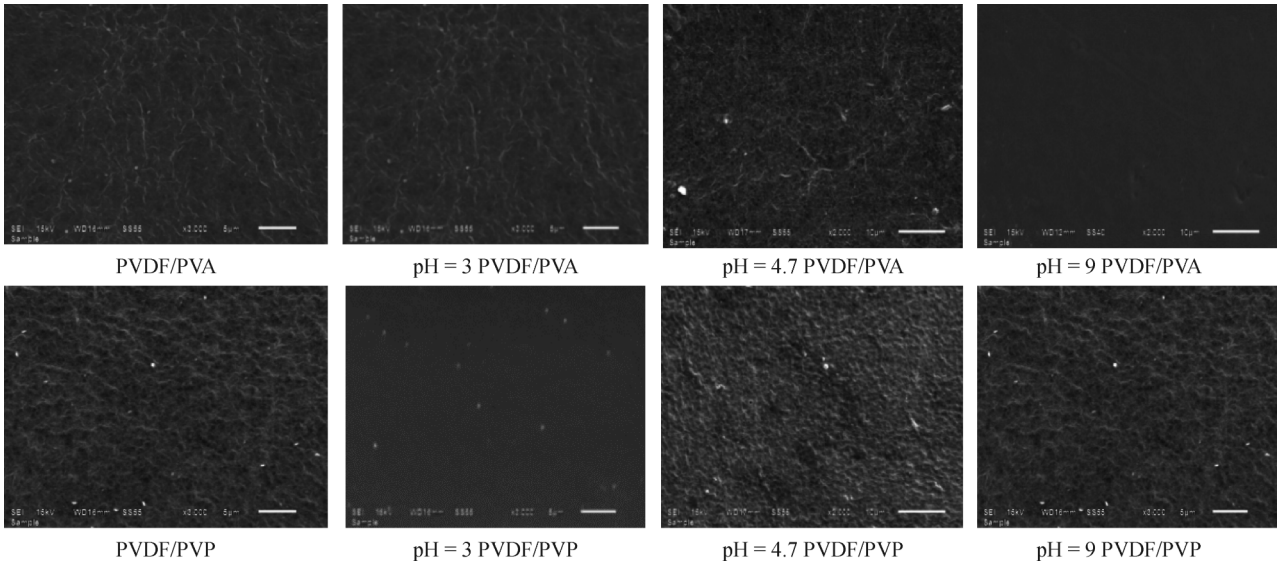

Fig. 6 The surface SEM images of membranes fouled by BSA solutions (Experimental conditions: test temperature, room temperature; Filtration time: 2 h)

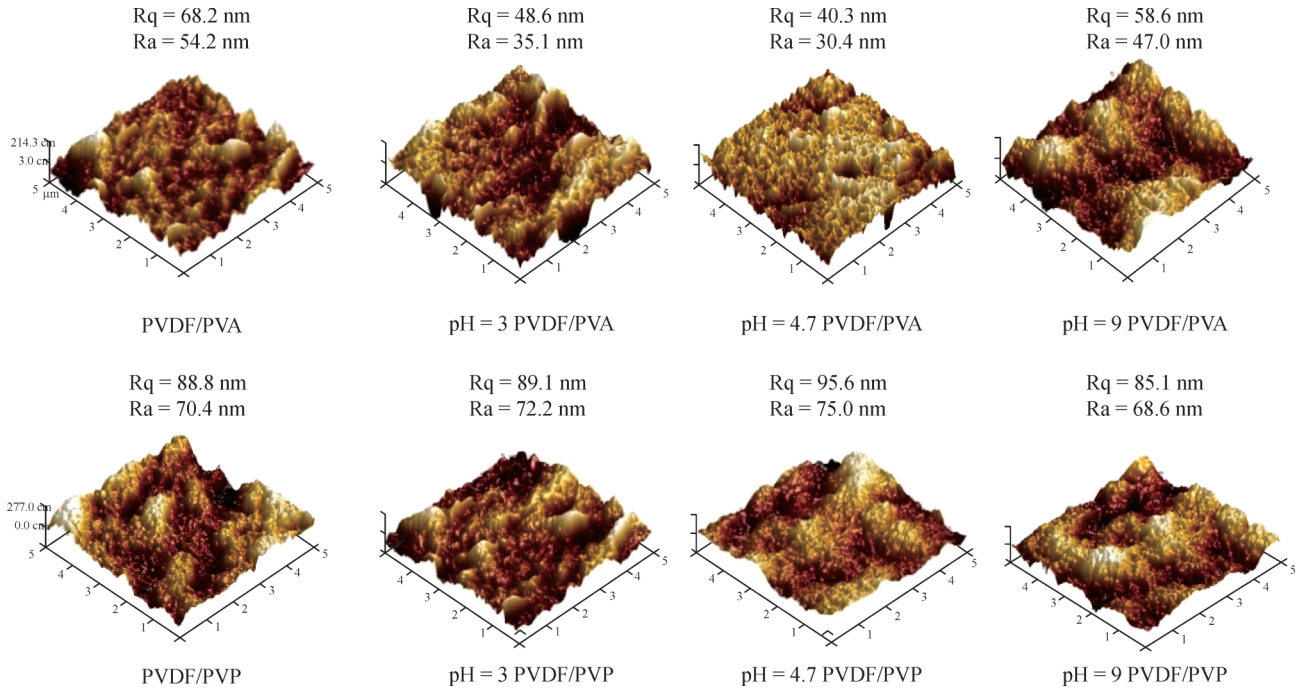

Fig. 7 The 3-dimensional AFM images of BSA fouled membranes (Experimental conditions: test temperature, room temperature; Filtration time: 2 h)

were fouled by BSA solution at pH 9 were similar. Therefore, the degree of membrane fouling causing by BSA solution under alkaline conditions was the lightest.

3.6 XDLVO theory of BSA fouling behavior in PVDF/PVA and PVDF/PVP membranes

Table 4 shows the average contact angles of PVDF/PVA and PVDF/PVP membranes and BSA. The θ_W of BSA has the highest value at pH 4.7, and the value under acidic conditions is higher than under alkaline conditions.

Table 4 also shows the electron donor component of surface tension (γ_i^-) and the electron acceptor component of surface tension (γ_l^+) for PVDF/PVA and PVDF/PVP membranes, and for BSA. The γ_i^- values of BSA were much higher than the γ_l^+ values, indicating that BSA was a stronger electron donor component. This is a typical characteristic of a hydration protein and the strong electron donor properties were attributed to the surface negative charge and the fact that it contained groups exposed on the protein surface. The γ_i^- values of BSA increase with increasing pH, whereas the γ_l^+ values decrease with increasing pH. This may be caused by the deprotonation of surface groups. When the pH is reduced, the property of being an electron donor is still dominant. The γ^{LW} of BSA has the highest value at pH 4.7. The deprotonation of surface groups did not have a significant impact on γ^{LW} values. This phenomenon may be related to LW interac-

Table 4 The contact angles, surface tension components and parameters ($mJ \cdot m^{-2}$) of membrane and BSA

Types	pH	θ_W/(°)	θ_D/(°)	θ_G/(°)	γ_l^+	γ_i^-	γ^{AB}	γ^{LW}	γ^{TOT}
PVDF/PVA	3	67.21 (± 0.15)	42.05 (± 0.11)	50.76 (± 0.31)	0.23	25.70	4.86	34.16	39.02
	4.7	67.70 (± 0.37)	46.30(± 0.52)	57.93(± 0.55)	0.69	13.91	6.20	36.70	42.90
	9	62.72 (± 0.29)	43.54 (± 0.17)	51.75 (± 0.16)	1.31	11.63	7.81	39.79	47.60
PVDF/PVP	3	84.40 (± 0.35)	47.80 (± 0.24)	59.10 (± 0.18)	0.65	7.84	4.51	30.51	35.02
	4.7	80.77 (± 0.51)	60.91 (± 0.67)	69.42 (± 0.12)	0.91	6.81	4.98	28.58	33.56
	9	73.91 (± 0.27)	52.82 (± 0.26)	63.00 (± 0.57)	0.96	10.50	6.35	33.74	40.09
BSA	3	76.59 (± 0.29)	37.16 (± 0.31)	66.95 (± 0.15)	0.07	7.09	1.41	40.96	42.37
	4.7	77.16 (± 0.24)	37.56 (± 0.18)	67.41 (± 0.28)	0.06	7.08	1.30	42.20	43.50
	9	72.43 (± 0.13)	34.17 (± 0.25)	65.64 (± 0.34)	0.02	10.60	0.92	40.83	41.75

Note: θ_W, θ_D and θ_G are the contact angle measured by ultrapure water, diiodomethane and glycerol. Data in the table are measured average of 5 times.

Table 5 PVDF UF membranes-BSA interfacial free energies of adhesion and BSA-BSA interfacial free energies of adhesion ($mJ \cdot m^{-2}$)

membranes	pH	ΔG_{mlf}^{LW}	ΔG_{mlf}^{AB}	ΔG_{mlf}^{AD}	ΔG_{flf}^{LW}	ΔG_{flf}^{AB}	ΔG_{flf}^{co}
PVDF/PVA	3	−5.09	−32.90	−37.99	−4.16	−20.91	−25.07
	4.7	−5.29	−37.91	−43.20	−4.91	−22.81	−27.72
	9	−4.24	−28.27	−32.51	−1.69	−19.64	−21.33
PVDF/PVP	3	−2.49	−43.13	−45. 62	−2.67	−23.21	−25.88
	4.7	−4.43	−53.40	−57.83	−3.44	−23.13	−26.57
	9	−2.92	−36.19	−39.11	−2.68	−20.23	−22.91

tion changes with different polarizations (or dielectric constants) between solid and solvent. The highly hydrated protein has a similar polarization to BSA–aqueous.

Table 5 shows the calculation results for the interfacial free energies of adhesion for the couples PVDF UF membranes–BSA and BSA–BSA. At the same pH condition, the absolute values of the AB component of free energy are much higher than the absolute values of the LW component of free energy in the interfacial free energies of membranes–BSA and BSA–BSA. The interfacial free energy values of PVDF/PVA membranes–BSA, which have good hydrophilicity, and of PVDF/PVP membranes–BSA, which have poor hydrophilicity, are negative, and the interaction between membrane and BSA is gravitation. Because the absolute values of PVDF/PVP membranes–BSA were higher than the values for PVDF/PVA membranes–BSA, BSA adhered much more easily to the surface of the PVDF/PVP membrane. For this reason, the adhesion force of PVDF/PVP membranes–BSA was stronger than that for PVDF/PVA membranes–BSA in AFM measurements and this is also the reason for the faster flux decline rate of the PVDF/PVP membrane in the filtration experiment. This is consistent with the results of HA research [26]. In addition, the absolute value of PVDF UF membranes–BSA interfacial free energies of adhesion (ΔG_{mlf}^{AD}) was the highest at pH 4.7. Therefore, at this pH, BSA has the largest fouling trends on PVDF/PVA and PVDF/PVP membranes. At pH 9, BSA has the lightest fouling trends on PVDF/PVA membranes.

Table 5 also shows that the BSA–BSA interfacial free energies of adhesion were similar for different kinds of membrane materials under the same pH conditions, but when the solution pH was 4.7, the BSA–BSA interfacial free energies of adhesion were much higher than at pH 9, and slightly higher than at pH 3. This phenomenon might have been related to the hydrogen ions on the BSA surface dissociating, the zeta potential closing to zero and the particle size of BSA being the smallest, which resulted in a tendency toward clogging and more serious membrane fouling. In addition, under acidic conditions, basic residues and hydrogen ions at the BSA surface are fully associative, and the particle size was smallest. In contrast, under alkaline conditions, BSA molecules dissociated while the particle size increased. Therefore, BSA caused more membrane fouling under acidic conditions than under the alkaline condition investigated here.

Under different pH conditions, the results calculated by the XDLVO theory reveal the order of the AB components of free energy (ΔG_{mlf}^{AB}) that play dominant roles in pH 9>pH 3>pH 4.7 during the adhesion process between the membranes and BSA, and show that the interface gravitational was the strongest at the pH 4.7, while interface gravitational weakened at pH 9. During the adhesion process between BSA and BSA, ΔG_{flf}^{CO} had the lowest value when the solution pH was 4.7.

4 Conclusions

At alkaline pH, the flux decline rates for PVDF/PVA and PVDF/PVP membranes were the lowest, and the membrane fouling was the lightest. But under acidic pH conditions, the flux through the membranes declined rapidly. When the pH was 4.7, the flux decline rate of the two membrane materials was increased. At the same pH condition, the adhesion force PVDF/PVA membrane–BSA was smaller than that of the PVDF/PVP membrane–BSA, illustrating that the more hydrophilic the membrane, the better its antifouling ability. The adhesion force of BSA–BSA-fouled membranes was similar for PVDF/PVA and PVDF/PVP membranes. These show that elimination of the membrane–BSA adhesion force is important in controlling the protein fouling of membranes.

The XDLVO theory shows that the Lewis acid–base interaction plays a dominant role in the occurrence of the membrane fouling and can affect it. For the same membrane, the pH values of the BSA solution could have a significant impact on the process of membrane fouling by changing the AB component of free energy.

Acknowledgements Financial support for this study was provided by the National Natural Science Foundation of China (Grant No. 51278408), the Shaanxi Province Science and Technology Innovation Projects (No. 2013KTCL03-16), Shaanxi Province Science and Technology Youth Star Project (Grant No. 2014KJXX-65) and the innovative research team of Xi'an University of Architecture and Technology.

Electronic Supplementary Material Supplementary material is available in the online version of this article at http://dx.doi.org/10.1007/s11783-016-0855-9 and is accessible for authorized users.

Nomenclature

J water flux ($L \cdot m^{-2} \cdot h^{-1}$)

J_0 pure water flux ($L \cdot m^{-2} \cdot h^{-1}$)

θ contact angle (deg)

θ_w contact angle measured by ultrapure water (deg)

θ_D contact angle measured by diiodomethane (deg)

θ_G contact angle measured by glycerol (deg)

LW Lifshitz–van der Waals interactions

AB polar or Lewis acid–base interactions

EL electrostatic double layer interactions

ΔG^{LW} LW component of free energy ($mJ \cdot m^{-2}$)

ΔG^{AB} AB component of free energy ($mJ \cdot m^{-2}$)

ΔG^{EL} EL component of free energy ($mJ \cdot m^{-2}$)

γ^{LW} LW component of surface tension ($mJ \cdot m^{-2}$)

γ_l^+ electron acceptor component of surface tension ($mJ \cdot m^{-2}$)

γ_i^- electron donor component of surface tension ($mJ \cdot m^{-2}$)

γ^{TOT} total component of surface tension ($mJ \cdot m^{-2}$)

ΔG^{AD}_{mlf} membrane–BSA interfacial free energy of adhesion ($mJ \cdot m^{-2}$)

ΔG^{CO}_{flf} BSA–BSA interfacial free energy of adhesion ($mJ \cdot m^{-2}$)

Subscripts

m membrane

l liquid environment

f foulant

References

1. Shannon M A, Bohn P W, Elimelech M, Georgiadis J G, Mariñas B J, Mayes A M. Science and technology for water purification in the coming decades. Nature, 2008, 452(7185): 301–310
2. Wang L, Wang X. Study of membrane morphology by microscopic image analysis and membrane structure parameter model. Journal of Membrane Science, 2006, 283(1–2): 109–115
3. Fan X, Tao Y, Wei D, Zhang X, Lei Y, Noguchi H. Removal of organic matter and disinfection by-products precursors in a hybrid process combining ozonation with ceramic membrane ultrafiltration. Frontiers of Environmental Science & Engineering, 2015, 9(1): 112–120
4. Mo H, Tay K G, Ng H Y. Fouling of reverse osmosis membrane by protein (BSA): effects of pH, calcium, magnesium, ionic strength and temperature. Journal of Membrane Science, 2008, 315(1–2): 28–35
5. Dong B, Chen Y, Gao N, Fan J. Effect of pH on UF membrane fouling. Desalination, 2006, 195(1–3): 201–208
6. He H, Sui Q, Lu S, Zhao W, Qiu Z, Yu G. Effect of effluent organic matter on ozonation of bezafibrate. Frontiers of Environmental Science & Engineering, 2015, 9(6): 962–969
7. Wang Q, Wang Z, Wu Z. Effects of solvent compositions on physicochemical properties and anti-fouling ability of PVDF microfiltration membranes for wastewater treatment. Desalination, 2012, 297: 79–86
8. Chang H, Qu F, Liu B, Yu H, Li K, Shao S, Li G, Liang H. Hydraulic irreversibility of ultrafiltration membrane fouling by humic acid: effects of membrane properties and backwash water composition. Journal of Membrane Science, 2015, 493: 723–733
9. Wang L, Miao R, Wang X, Lv Y, Meng X, Yang Y, Huang D, Feng L, Liu Z, Ju K. Fouling behavior of typical organic foulants in polyvinylidene fluoride ultrafiltration membranes: characterization from microforces. Environmental Science & Technology, 2013, 47 (8): 3708–3714
10. Ang W S, Elimelech M. Protein (BSA) fouling of reverse osmosis membranes: implications for wastewater reclamation. Journal of Membrane Science, 2007, 296(1–2): 83–92
11. She Q, Tang C Y, Wang Y N, Zhang Z. The role of hydrodynamic conditions and solution chemistry on protein fouling during ultrafiltration. Desalination, 2009, 249(3): 1079–1087
12. Wei L, Wang K, Kong X, Liu G, Cui S, Zhao Q, Cui F.Application of ultra-sonication, acid precipitation and membrane filtration for co-recovery of protein and humic acid from sewage sludge. Frontiers of Environmental Science & Engineering, 2016, 10(2), 327–335
13. Velasco C, Calvo J, Palacio L, Carmona J, Prádanos P, Hernández A. Flux kinetics, limit and critical fluxes for low pressure dead-end microfiltration: the case of BSA filtration through a positively charged membrane. Chemical Engineering Science, 2015, 129: 58–68
14. Ahmad B, Kamal M Z, Khan R H. Alkali-induced conformational transition in different domains of bovine serum albumin. Protein and Peptide Letters, 2004, 11(4): 307–315
15. Ho C C, Zydney A L. A combined pore blockage and cake filtration model for protein fouling during microfiltration. Journal of Colloid and Interface Science, 2000, 232(2): 389–399
16. Duclos-Orsello C, Li W, Ho C C. A three mechanism model to describe fouling of microfiltration membranes. Journal of Membrane Science, 2006, 280(1–2): 856–866
17. Sun X, Kanani D M, Ghosh R. Characterization and theoretical analysis of protein fouling of cellulose acetate membrane during constant flux dead-end microfiltration. Journal of Membrane Science, 2008, 320(1–2): 372–380
18. Ma B, Hu C, Wang X, Xie Y, Jefferson W A, Liu H, Qu J. Effect of aluminum speciation on ultrafiltration membrane fouling by low dose aluminum coagulation with bovine serum albumin (BSA). Journal of Membrane Science, 2015, 492: 88–94
19. Mosley L M, Hunter K A, Ducker W A. Forces between colloid particles in natural waters. Environmental Science & Technology, 2003, 37(15): 3303–3308
20. Zhang W, Stack A G, Chen Y. Interaction force measurement between *E. coli* cells and nanoparticles immobilized surfaces by using AFM. Colloids and Surfaces. B, Biointerfaces, 2011, 82(2): 316–324
21. Hashino M, Hirami K, Ishigami T, Ohmukai Y, Maruyama T, Kubota N, Matsuyama H. Effect of kinds of membrane materials on

membrane fouling with BSA. Journal of Membrane Science, 2011, 384(1–2): 157–165

22. Miao R, Wang L, Wang X, Lv Y, Gao Z, Mi N, Liu T. Preparation of a polyvinylidene fluoride membrane material probe and its application in membrane fouling research. Desalination, 2015, 357: 171–177
23. Derjaguin B. Theory of the stability of strongly charged lyophobic sols and the adhesion of strongly charged particles in solutions of electrolytes. Acta Physicochim. USSR, 1941, 14: 633–662
24. Verwey E J. Theory of the stability of lyophobic colloids. Journal of Physical Chemistry, 1947, 51(3): 631–636
25. Lin T, Lu Z, Chen W. Interaction mechanisms of humic acid combined with calcium ions on membrane fouling at different conditions in an ultrafiltration system. Desalination, 2015, 357: 26–35
26. Meng X, Tang W, Wang L, Wang X, Huang D, Chen H, Zhang N. Mechanism analysis of membrane fouling behavior by humic acid using atomic force microscopy: effect of solution pH and hydrophilicity of PVDF ultrafiltration membrane interface. Journal of Membrane Science, 2015, 487: 180–188
27. Meng X, Zhang H, Wang L, Wang X, Zhao L. Membrane fouling by secondary effluent of urban sewage and the membrane properties. Environmental Sciences, 2013, 34(5): 1822–1827
28. Brant J A, Childress A E. Assessing short-range membrane–colloid interactions using surface energetics. Journal of Membrane Science, 2002, 203(1–2): 257–273
29. Subramani A, Hoek E M. Direct observation of initial microbial deposition onto reverse osmosis and nanofiltration membranes. Journal of Membrane Science, 2008, 319(1–2): 111–125
30. van Oss C J, Chaudhury M K, Good R J. Monopolar surfaces. Advances in Colloid and Interface Science, 1987, 28(1): 35–64
31. Li J F, Xu Z L, Yang H. Microporous polyethersulfone membranes prepared under the combined precipitation conditions with non-solvent additives. Polymers for Advanced Technologies, 2008, 19 (4): 251–257
32. Feng C, Shi B, Li G, Wu Y. Preparation and properties of microporous membrane from poly (vinylidene fluoride-co-tetrafluoroethylene)(F2.4) for membrane distillation. Journal of Membrane Science, 2004, 237(1–2): 15–24
33. Saikia D, Kumar A. Ionic conduction in P(VDF-HFP)/PVDF–(PC + DEC)–$LiClO_4$ polymer gel electrolytes. Electrochimica Acta, 2004, 49(16): 2581–2589
34. Wang Y N, Tang C Y. Fouling of nanofiltration, reverse osmosis, and ultrafiltration membranes by protein mixtures: the role of interfoulant-species interaction. Environmental Science & Technology, 2011, 45(15): 6373–6379
35. Miao R, Wang L, Lv Y, Wang X, Feng L, Liu Z, Huang D, Yang Y. Identifying polyvinylidene fluoride ultrafiltration membrane fouling behavior of different effluent organic matter fractions using colloidal probes. Water Research, 2014, 55: 313–322